Orbital Constraints on Exoplanet Habitability

Zachery McBrearty

Level 4 Project, MPhys Physics with Astronomy

Supervisor: Dr Richard Wilman

Second Supervisor: Dr Craig Testrow

Department of Physics, Durham University

Submitted: March 7, 2024

A 1-D energy balance climate model is developed in order to investigate how changing certain orbital parameters can result in changes to a planet's habitability. Theoretical relationships between temperature, semimajoraxis, and eccentricity are derived from a 0-D energy balance model and are tested against the 1-D model and are found to be correct. A qualitative analysis of obliquity shows that there are optimal obliquities to minimise and maximise global temperature. The climates of exomoons orbiting gas giants are also investigated, including reflected light from the gas giant, eclipsing, and tidal heating. It is expected that these additional sources of heat move the habitable zones for the planet outwards.

CONTENTS

1. INTRODUCTION

A. Exoplanet and Exomoon detection

When the first exoplanet was discovered is up for debate depending on classification [1]. To give a summary: The first evidence for an exoplanet came in 1988 but was attributed to stellar activity. This was followed up later in 2003 and found to be a exoplanet. This confirmation happened many years after 1992 when the first exoplanets were found orbiting a pulsar via the variations in pulsar timings due to those exoplanets. However the intensity of radiation from these pulsars make life on these exoplanets impossible. Then the first potentially habitable exoplants were found in 1995; potentially habitable because they orbit a Sun-like star.

Exoplanets are now found in a variety of indirect and direct methods. Indirect methods include pulsar timing, radial velocity, astrometry, and gravitational lensing. Direct methods include transits and direct imaging via coronagraph. Direct and indirect methods have also been combined to find planets. For example Kepler-88c was discovered indirectly due to variation in the transit of Kepler-88b [2].

These methods can also be extended to find exomoons around exoplanets. The pulsar timing from an exoplanet has additional variations due to a exomoon [3] and it has been shown that nearby exomoons may be found using Kepler (or Kelper-class) photometry by analysing variations in transit timing signals [4].

More recently, it has been shown that exomoons with strong tidal heating could be brighter brighter than the exoplanet they orbit, so are easier to detect than exoplanets in some cases [5]. Further, the launch of the JWST has enabled the direct detection of earth-sized exomoons with economical use of observation time [6].

The culmination of all these methods is collated by the Encyclopaedia of Exoplanetary Systems [7] who report a total of 5641 exoplanets confirmed but no exomoons.

Reaching these exoplanets is a project for the far future, however current missions are building up to this auspicious goal. The one recent (and on going) mission is the Artemis Plan [8] which plans to build a Base Camp on the lunar surface and setup Gateway in lunar orbit. Additionally, the China National Space Administration also plan to return to the moon with the International Lunar Research Station [9]. Both these projects will allow for human settlement away from the Earth, and are vital in progressing further out into our own solar system and beyond.

B. Energy balance models

Analysing the habitability of exoplanets can be difficult. The Trappist-1 system is an excellent example. In the system seven Earth-like planets were found within the habitable zone of their host star [10]. However they are not habitable due to a mixture of being tidally-locked to the star and experiencing extreme solar winds which have probably stripped them of any atmosphere long ago [11, 12]. This suggests that modelling of an exoplanet's habitability requires modelling of the dynamic atmosphere,

One way to model the exoplanets is with an energy balance model, where incoming energy

(usually from a star) is equated to outgoing energy (usually blackbody emission). If no time dependence is considered then the 0-D Energy Balance Model (0DEBM) is

$$\pi r^2 S(1 - A) = 4\pi r^2 \sigma T^4, \tag{1}$$

where r is the radius of the planet, S is the incoming solar radiation (insolation) which is reduced by the albedo of the planet A. The blackbody term is given by the Stefan-Boltzmann constant σ and the temperature of the planet T. This model does not resolve the planet's surface, and comes with a variety of assumptions such as energy being distributed equally over the entire planet's surface. This assumption implies that the planet is not tidally locked and has good diffusion mechanisms to spread out heat.

While this 0DEBM is powerful, there are limitations. The temperature produced is an average over time which means extreme temperatures are ignored. Different latitude bands experience different amounts of insolation depending on time and obliquity, thus the assumption of even energy distribution is not entirely valid. This is especially apparent on the Earth where the poles have much lower temperatures (i.e. freezing) than the equator.

These problems can be addressed with a 1-D Energy Balance Climate Model (1DEBCM). The 1DEBCM is given in latitude, λ, coordinates as

$$C(\lambda, T)\frac{\partial T(t, \lambda)}{\partial t} = D\left[\frac{\partial^2 T(t, \lambda)}{\partial \lambda^2} - \tan\lambda \frac{\partial T(t, \lambda)}{\partial \lambda}\right] + S(\lambda, t)(1 - A(T)) - I(T), \tag{2}$$

Where C is the heat capacity for a latitude band, D is the diffusion constant regulating the horizontal transport of heat between latitude bands, I is the generalised IR emission for a latitude band. The other terms are the same as the 0DEBM. Forms for these functions are given in Section 4.

The 1DEBCM can be derived from the heat equation (see Section 2) and was originally developed by North and Coakley 1979 (NC79) [13] to study the Earth. It was then further applied by Williams and Kasting 1997 (WK97) [14] to study obliquity dependent habitability and then by Spiegel et al in 2008 (SMS08) [15] and 2009 [16] to study quantify habitability and then study obliquity dependent habitability. Spiegel's work was furthered by Dressing et al 2010 [17] where eccentricity dependent habitability was investigated.

C. Habitability

SMS08 quantifies habitability in 3 main ways. The first is the time-averaged habitability, f_{time}, which is given in their eqn. (6) as

$$f_{\text{time}}(q, \lambda) = \frac{1}{P}\int_0^P H(q, \lambda, t)dt, \tag{3}$$

where P is the length of the year for the model in question and $H(q, \lambda, t)$ is a habitability function; 1 if the temperature is habitable, 0 if not. The second is the area-weighted habitability, f_{area}, which is given in their eqn. (7) as

$$f_{\text{area}}(q, t) = \frac{1}{2}\int_{-\pi/2}^{\pi/2} H(q, \lambda, t)\cos(\lambda)d\lambda, \tag{4}$$

where the area weighting occurs as each latitude band has unequal area. Finally the combination of these two measures results in the total habitability, f_{total}, given in their eqn. (8) as

$$f_{\text{total}}(q) = \frac{1}{2P} \int_{-\pi/2}^{\pi/2} \int_0^P H(q, \lambda, t) dt \cos(\lambda) d\lambda, \tag{5}$$

where in all three cases the semimajor axis a has been replaced by a generalised parameter (or set of parameters) q. This paper uses the discrete form of these equations in Section 3 in order to both quantify when a model has reached an stable average (i.e. equilibrium) temperature and for quantifying the habitability of a model which varies in time and latitude. Also in given in Section 3 are the two habitability functions used throughout this paper.

The 1DEBCM can be used to ...

exomoons

2.   1-D ENERGY BALANCE CLIMATE MODEL

The EBCM can be derived from the standard heat equation given by

$$\frac{\partial T}{\partial t} = \alpha \nabla^2 T, \tag{6}$$

where $T(t, r, \theta, \phi)$ is the temperature at time t, radius r, co-latitude θ, and longitude ϕ. The constant α is related to the heat capacity and diffusion rate of the system. Expanding the laplacian in spherical coordinates the equation becomes

$$\frac{\partial T}{\partial t} = \alpha \left[\frac{1}{r} \frac{\partial^2}{\partial r^2}(rT) + \frac{1}{r^2 \sin \theta} \frac{\partial}{\partial \theta} \left(\sin \theta \frac{\partial T}{\partial \theta} \right) + \frac{1}{r^2 \sin^2 \theta} \frac{\partial^2 T}{\partial \theta^2} \right]. \tag{7}$$

The EBCM is arrived at by first letting $T(t, r, \theta, \phi) = T(t, \lambda)$, with latitude $\lambda = \pi - \theta$. Thus the equation simplifies to

$$\begin{aligned}
\frac{\partial T}{\partial t} &= \frac{\alpha}{r^2 \sin \theta} \frac{\partial}{\partial \theta} \left(\sin \theta \frac{\partial T}{\partial \theta} \right) \\
&= \frac{\alpha}{r^2} \left(\frac{\partial^2 T}{\partial \lambda^2} - \tan \lambda \frac{\partial T}{\partial \lambda} \right).
\end{aligned} \tag{8}$$

The original equation can be recovered by defining $\alpha/r^2 \equiv D/C$ for diffusion constant D and heat capacity C. Then adding incoming solar radiation S (insolation), which is reduced by planetary albedo A, and outgoing IR-emission I to the PDE. Thus the original form of the 1D EBCM in eqn. (2) is recovered.

A.   Discretisation of the climate model

Numerically integrating the EBCM requires the derivatives to be discretised. Spatially the planet can be split into S latitude bands, separated by

$$\Delta \lambda = \frac{\pi^{\text{rad}}}{S - 1} = \frac{180°}{S - 1}, \tag{9}$$

with spatial indexing of each band from $m = 0, 1, \ldots, S - 1$. Similarly, a temporal indexing of $n = 0, 1, \ldots$ is used to discretise time in steps of Δt. Thus T_n^m is the temperature at the mth timestep for the nth latitude band.

The spatial derivatives can then be approximated by the central difference and second order central difference:

$$\frac{\partial T_n^m}{\partial \lambda} = \frac{T_n^{m+1} - T_n^{m-1}}{2\Delta\lambda}, \tag{10}$$

$$\frac{\partial^2 T_n^m}{\partial \lambda^2} = \frac{T_n^{m+2} - 2T_n^m + T_n^{m-2}}{(2\Delta\lambda)^2}, \tag{11}$$

and the temporal derivative can be approximated as a forward difference,

$$\frac{\partial T_n^m}{\partial t} = \frac{T_{n+1}^m - T_n^m}{\Delta t}, \tag{12}$$

with numerical stability analysed in appendix A. Evolving the EBCM is performed by solving eqn. (12) for T_{n+1}^m in terms of the parameter and temperature values at timestep n.

However, a problem arises at the edges of the model as $m = -2, -1, S, S+1$ are not defined. To fix this the derivatives at $m = 0$ ($m = S - 1$) are discretised as forward then backward (backward then forward) derivatives. By imposing that $\partial T_n^{m=0,S-1}/\partial\lambda = 0$, the second order derivatives then reduce to

$$\frac{\partial^2 T_n^{m=0}}{\partial \lambda^2} = \frac{1}{\Delta\lambda}\left(\frac{\partial T_n^{m=1}}{\partial\lambda} - \frac{\partial T_n^{m=0}}{\partial\lambda}\right) \qquad = \frac{T_n^{m=1} - T_n^{m=0}}{(\Delta\lambda)^2} \tag{13}$$

$$\frac{\partial^2 T_n^{m=S-1}}{\partial \lambda^2} = \frac{1}{\Delta\lambda}\left(\frac{\partial T_n^{m=S-1}}{\partial\lambda} - \frac{\partial T_n^{m=S-2}}{\partial\lambda}\right) = \frac{T_n^{m=S-2} - T_n^{m=S-1}}{(\Delta\lambda)^2}. \tag{14}$$

Furthermore, the treatment imposed for the $m = 1$ and $m = S - 2$ second order derivatives is much the same, using central-backward and central-forward derivatives respectively.

3. METHOD

Analysing the data produced requires the use of area-weighted averaging and time averaging from SMS08. The original equations are given as continuous integrals, but are discretised in a similar way to the derivatives in 2 A. Thus the time averaging, area-weighted averaging, and total averaging are given by

$$\begin{aligned} Q_{p \to q}^m &= \frac{\sum_{n=p}^{q} Q_n^m \Delta t}{\sum_{n=p}^{q} \Delta t} \\ &= \frac{\sum_{n=p}^{q} Q_n^m}{t_q - t_p} \end{aligned}, \tag{15}$$

$$\bar{Q}_n = \sum_{m=0}^{S-1} Q_n^m F^m = \sum_{m=0}^{S-1} \frac{1}{2} Q_n^m \cos(\lambda_m)\Delta\lambda, \tag{16}$$

$$\bar{Q}_{p \to q} = \frac{\sum_{n=p}^{q} \sum_{m=0}^{S-1} Q_n^m \cos(\lambda_m)\Delta\lambda}{2(q - p)}, \tag{17}$$

respectively, with the time averaging happening between a time t_p and t_q. These averages can now be used to evaluate if a model has reached an equilibrium temperature and what the average habitability of a planet is.

A model is said to reach an equilibrium temperature when the average temperature between 2 averaging periods divided by the average temperature over both periods is less than some tolerance ϵ:

$$\frac{\bar{T}_{p \to q} - \bar{T}_{q \to r}}{\bar{T}_{p \to r}} < \epsilon. \tag{18}$$

Typically the averaging occurs over an orbital period (i.e. local year), so the equilibrium temperature is when there are no significant variations in temperature between two consecutive orbits. The value of ϵ chosen directly influences how long the model must be run to reach an equilibrium. In most cases a value of $\epsilon = 10^{-3}$ is used and results in equilbrium times of between 20 and 150 years depending on model parameters. It is worth noting for some plots that a value of $\langle T \rangle = -1$ means the model did not reach an equilbrium temperature within the evolution time and value of ϵ. This $\langle T \rangle = -1$

The classical habitability function is the Liquid Water Requirement (LWR) given by

$$H_{\text{LWR}}(T) = \begin{cases} 1 & 0°\text{C} \leq T \leq 100°\text{C} \\ 0 & \text{Otherwise} \end{cases}, \tag{19}$$

Thus a temperature is habitable if it is between the boiling and melting points of water.

An alternative is motivated by the limits of human endurance, thus is called Human Compatibility (HC). If a human's core temperature is raised above $35°$C then enzymes esssential for life denature and breakdown. This does not mean temperatures above this are lethal as humans can regulate temperature by sweating. The wet bulb temperature is defined by wrapping a thermometer bulb with a wet cloth. It is designed to take the humidity and ambient temperature into account, essentially mimicking the internal temperature of a human. Thus a wetbulb temperature of $35°$C is lethal if prolonged.

This climate model does not calculate humidity, thus a conservative temperature at which habitability reduces is taken to be $30°$C:

$$H_{\text{HC}}(T) = \begin{cases} 1 & 0°\text{C} \leq T \leq 30°\text{C} \\ 0 & \text{Otherwise} \end{cases}, \tag{20}$$

with the additional constraint that temperatures greater than $40°$C or less than $-10°$C in a latitude band sets the habitability of the band to 0 for all time.
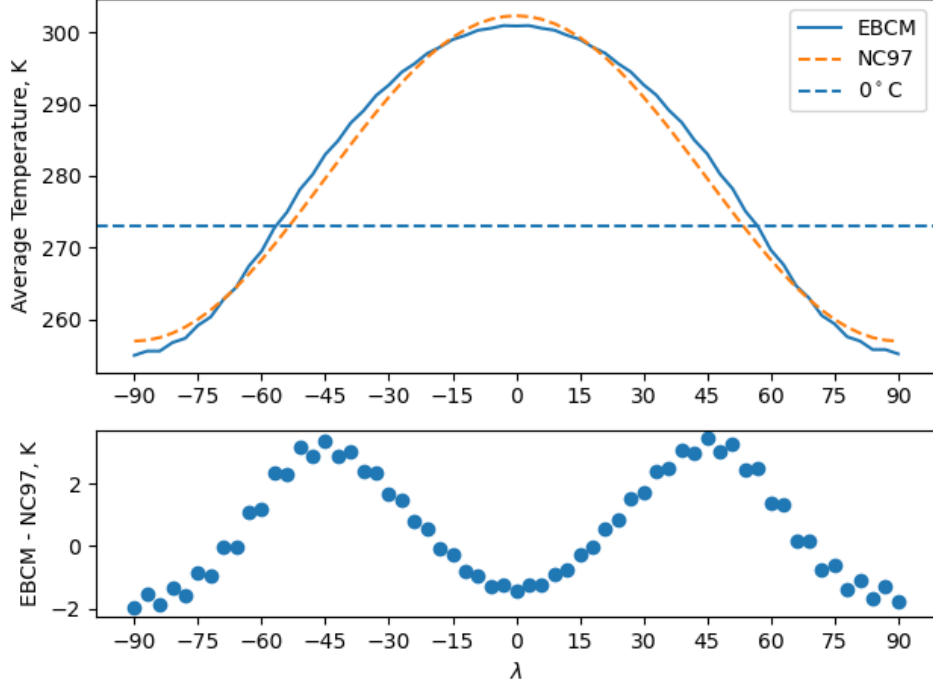
4.   EARTH-LIKE MODEL

In order to investigate the Earth and Earth-like planets, the parameters and functions which define the Earth must be established. In this analysis the forms of the model functions are taken from Williams and Kastings (WK97) [14], and the model is compared against the model from North and Coakley 1979 (NC79) [13] which has been time-averaged as follows.

The first 3 terms of the NC79 model are given in their eqn. (4) as

$$T(\lambda, t)[°\text{C}] = 14.2 + 15.5 \cos(\omega t + \phi) P_1(\sin \lambda) - 30.2 P_2(\sin(\lambda)), \tag{21}$$

Semimajor axis a, au	Eccentricity e	Obliquity δ, deg	No. spatial nodes S	Timestep Δt, days	Land fraction type
1	0.0167	23.5	61	1	Uniform 70% Ocean

TABLE I: A summary of the default parameters for the Earth-like model. A 'Uniform' land fraction indicates that the model has the same ratio of land to ocean across the entire planet. The odd number of spatial nodes means there is a true equator with $\lambda = 0$ as well as poles with $\lambda = \pm 90°$

FIG. 1: The 10-year-averaged temperature distribution of the Earth-like model given in I. Overlaid on the fit is the time averaged Earth model from North and Coakley's 1979 paper [13]. The diffusion parameter D_0 in eqn. (23) was varied to give the best agreement between the two models. The value found to work best is $D_0 = 0.56 \, \text{Wm}^{-2}\text{K}^{-1}$.

where P_i is the ith Legendre polynomial. The time-averaged temperature is found when averaging eqn. (21) over a year period,

$$
\begin{aligned}
T(\lambda)[\text{K}] &= 14.2 + 273 - 30.2(3\sin^2(\lambda) - 1)/2 \\
&= 302.3 - 45.3\sin^2(\lambda),
\end{aligned} \tag{22}
$$

where the temperature has been converted to Kelvin, and the second legrendre polynomial is expanded as $P_2(x) = (3x^2 - 1)/2$. The average of $\cos(\omega t + \phi)$ over an period $T = 2\pi/\omega$ is 0, so the first legendre polynomial is not needed.

The diffusion varies with orbital and atmospheric parameters as,

$$
\frac{D}{D_0} = \frac{p}{p_0}\frac{c_p}{c_{p,0}}\left(\frac{m}{28}\right)^{-2}\left(\frac{\Omega}{1 \, \text{day}^{-1}}\right)^{-2} \tag{23}
$$

where $D_0 = 0.56 \, \text{Wm}^{-2}\text{K}^{-1}$ is from fitting to eqn. 22 as shown in Fig. 1. The atmospheric
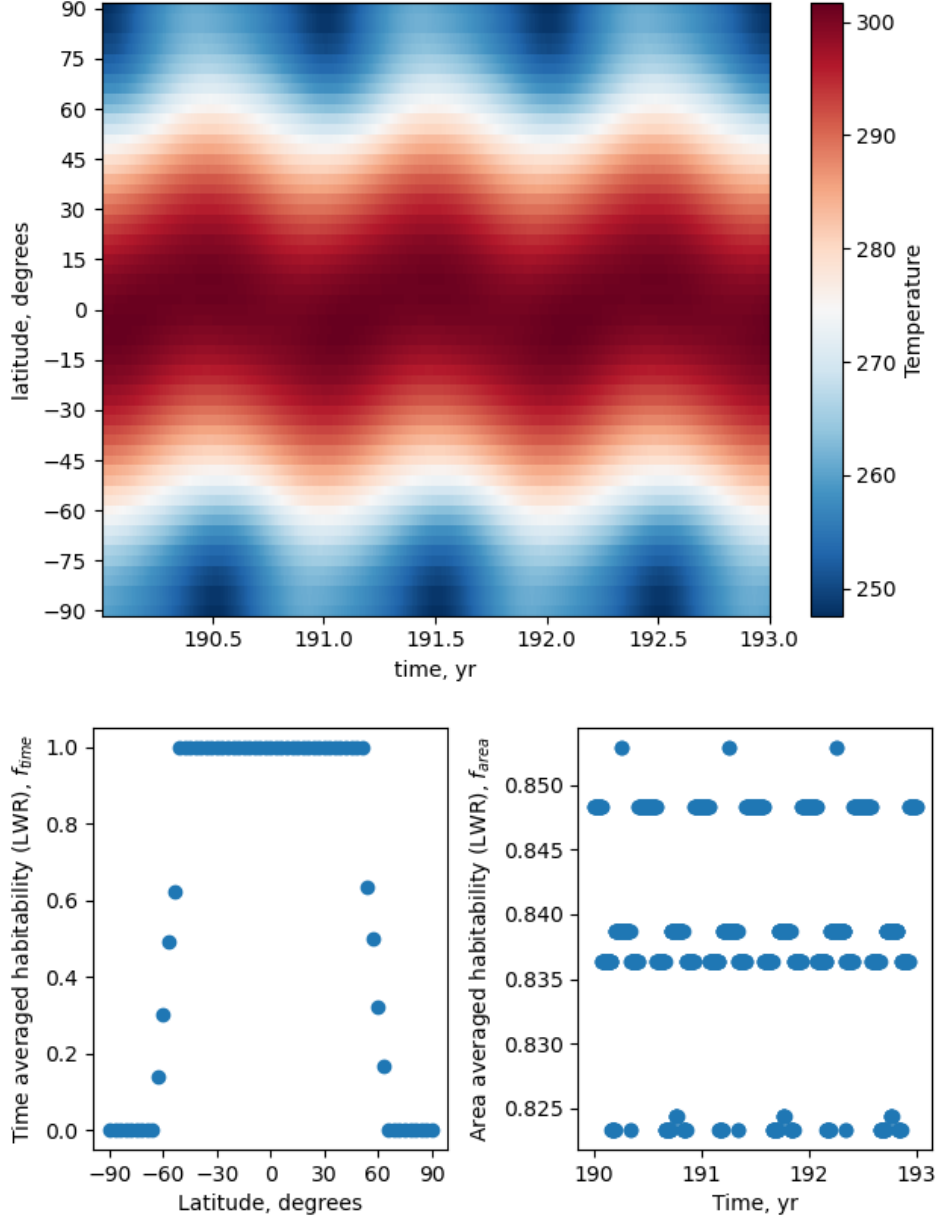
FIG. 2: Top: The temperature distribution for the Earth model with parameters given in Table I. The time range is for 2 years, showing the periodicity of the seasons in the model. Bottom: The temperature distribution processed with the LWR habitability (eqn. (19)) and then averaged over time (left) or area (right).

pressure p is relative to $p_0 = 101$ kPa. The heat capacity c_p of the atmosphere is relative to $c_{p,0} = 1 \times 10^3$ g^{-1}K^{-1}. Average mass of particles in the atmosphere is given by m and is relative to the Nitrogen molecule. Rotation rate of the planet Ω is relative to Earth's 1 rotation per day. These parameters can be extended to be time variable, such as having CO$_2$ emissions increase pressure, change heat capacity, and change mass of particles. However this paper only considers varying the rotation rate of the planet.

Heat capacity, $C(\lambda, T)$, varies with latitude through the ocean-land fraction, $f_o(\lambda)$, and with

temperature through the ice-ocean fraction, $f_i(T)$, as

$$C(\lambda, T) = (1 - f_o(\lambda))C_{\text{land}} + f_o(\lambda)((1 - f_i(T))C_{\text{ocean}} + f_i(T)C_{\text{ice}}(T)), \tag{24}$$

Where $C_{\text{land}} = 5.25 \times 10^6 \text{ Jm}^{-2}\text{K}^{-1}$ and $C_{\text{ocean}} = 40 \times C_{\text{land}}$ are constant, and

$$C_{\text{ice}}(T) = \begin{cases} 9.2 C_{\text{land}} & T \geq 263\text{K} \\ 2.0 C_{\text{land}} & T < 263\text{K}, \end{cases} \tag{25}$$

which encapsulates the additional energy requirements of the heat of fusion, and expects that the water would be entirely frozen below $-10°$C. The ratio of ocean to land for the Earth is 70% ocean to 30% land. This model assumes this ratio is uniform and constant across the entire planet, thus $f_o = 0.7$. This is a simplification as the Earth has an uneven distribution of land and ocean, with most of the land in the northern hemisphere.

With definitions of diffusion and heat capacity, the timestep and latitude step which are numerically stable can be calculated. To do this the EBCM is investigated with a plane wave solution and boundaries on the timestep and latitude step are found. The explicit calculation of this is shown in appx. A, with the result that, for constant diffusion and timestep, a lower heat capacity requires a larger latitude step. The default values for the model are then taken as a timestep of $\Delta t = 1$ day and $S = 61$ latitude nodes ($\Delta \lambda = 3°$ separation)/ These parameters give good resolution while being completely numerically stable. For planets with $f_o = 0$ a lower value of $S = 31$ is chosen as it is stable for the land-only heat capacity value.

WK97 provides three sets of IR-emission and Albedo functions. Following the example of SMS08 and Dressing et al 2010 (here on Dressing10) [17] the second set of IR and Albedo functions which are given by

$$I(T) = I_2(T) = \frac{\sigma T^4}{1 + 0.5925(T/273\text{K})^3} \tag{26}$$

$$A(T) = A_2(T) = 0.525 - 0.245 \tanh\left(\frac{T - 268\text{K}}{5}\right), \tag{27}$$

are used in all models. This IR-emission is a blackbody radiation term (numerator) damped by the optical thickness of the atmosphere (denominator) which is roughly equivalent to the greenhouse gas effect due to water vapour content in the air. The albedo function is a smooth scaling from low reflectivity of land and forest to high reflectivity due to ice and snow.

The insolation function, S, is defined in WK97 as the day averaged incident (based on latitude) radiation from the sun,

$$S(\lambda, t) = \frac{q_0}{\pi}\left(\frac{1 \text{ au}}{r(t)}\right)^2 (H(t)\sin\lambda\sin\delta(t) + \cos\lambda\cos\delta(t)\sin H(t))$$

where $q_0 = 1360 \text{ Wm}^{-2}$ is the insolation from the Sun, $r(t)$ is the distance from the Sun, $\cos H(t) = -\tan\lambda\tan\delta(t)$ is the radian half-day length with $0 < H < \pi$, and $\delta(t)$ is the solar declination defined by

$$\sin\delta(t) = -\sin\delta_0\cos(L_s(t) + \pi/2)$$

where δ_0 is the obliquity of the planet and $L_s(t) = \omega t$ is orbital longitude from an orbital angular velocity found by Kepler's laws. It is important to average over a day insolation as the

model does not have a longitude dimension, so cannot account for uneven distribution of the insolation, for example in the case of a tidally locked planet.

The distance from the Sun is variable due to eccentricity. For a 2-body system this distance can be calculated through an iterative method as follows

$$r = a(1 - e \cos E), \tag{28}$$

where a and e are semimajor axis and eccentricity respectively, and the eccentricity anomaly E is given by iteration

$$\begin{aligned} E_0 &= M \\ E_{i+1} &= E_i + \frac{M + e \sin E_i - E_i}{1 - e \cos E_i}, \end{aligned} \tag{29}$$

where $M = 2\pi(t + t_0)/T$ for a temporal offset t_0 and period of the orbit T. The error in this function inceases with higher e but reduces with additional iterations. Three iterations with an eccentricity of 0.9 gives an error in E of 5% (compared to 100 iterations), which is a good compromise between computation time and accuracy, especially as $e = 0.9$ is the upper bound for eccentricities considered.

The temperature distribution for the Earth model is shown in Fig. 2 for 2 years after 190 years of evolution. There is clear periodicity in the model corresponding clearly with the seasonal variations experienced by the Earth.

Also shown is the LWR habitability of this temperature data which has been time averaged with eqn. (15) and area averaged with eqn. (16). The time and area averaged habitability is $H_{\text{Earth}} = 0.84$, meaning that the Earth is, when using LWR, 84% habitable. When using HC habitability this value is slightly reduced but the same to two significant figures.

The time averaged habitability shows how the the equator is habitable all year around. The poles are uninhabitable year round. Between $65°$ to $45°$ the habitability decreases linearly, representative of the variablity of the frost line.

The area averaged habitability changes in steps as each discrete latitude band becomes habitable or uninhabitable. It is periodic but difficult to predict within each year.

5. EARTH-LIKE EXOPLANETS

### A. Investigating time-averaged solar flux

General temperature relations for a planet can be found from the 0D EBCM. Time averaged insolation of an planet in an elliptical orbit is given by

$$S = \langle F \rangle = \frac{q_0}{a^2 \sqrt{1 - e^2}}, \tag{30}$$

where $q_0 = L_{\text{Sun}}/4\pi a_{\text{Earth}}^2 \approx 1360 \ \text{Wm}^{-2}$ is the bolometric solar flux for Earth, a and e are the semimajor axis and eccentricity respectively of the planet [19].

By subsituting this relation into equation (1), the temperature of a planet can be related to semimajor axis and eccentricity through

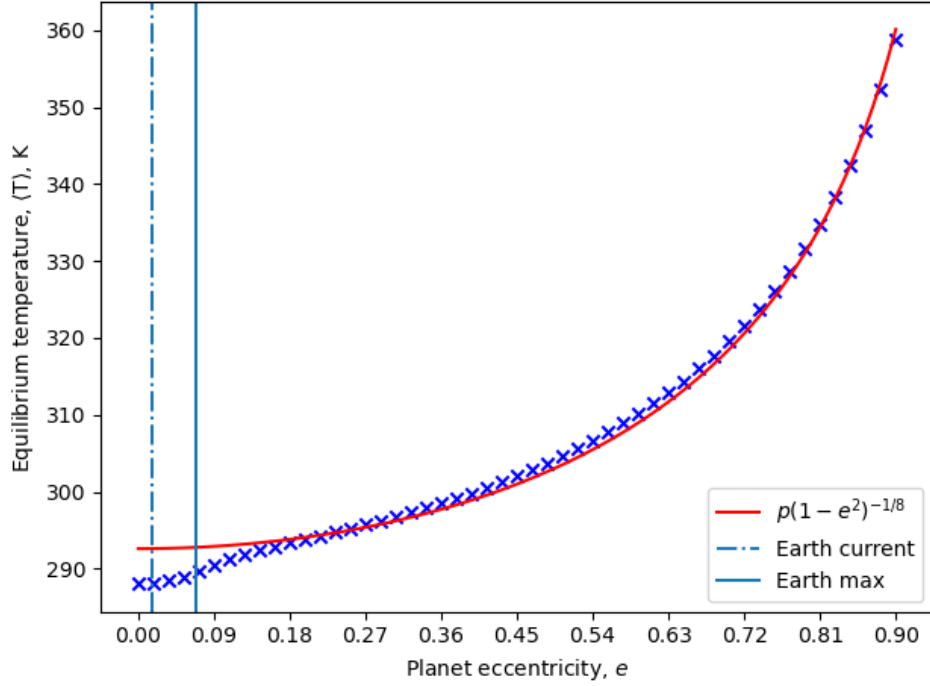$$T \propto a^{-\frac{1}{2}}(1 - e^2)^{-\frac{1}{8}}, \tag{31}$$

11
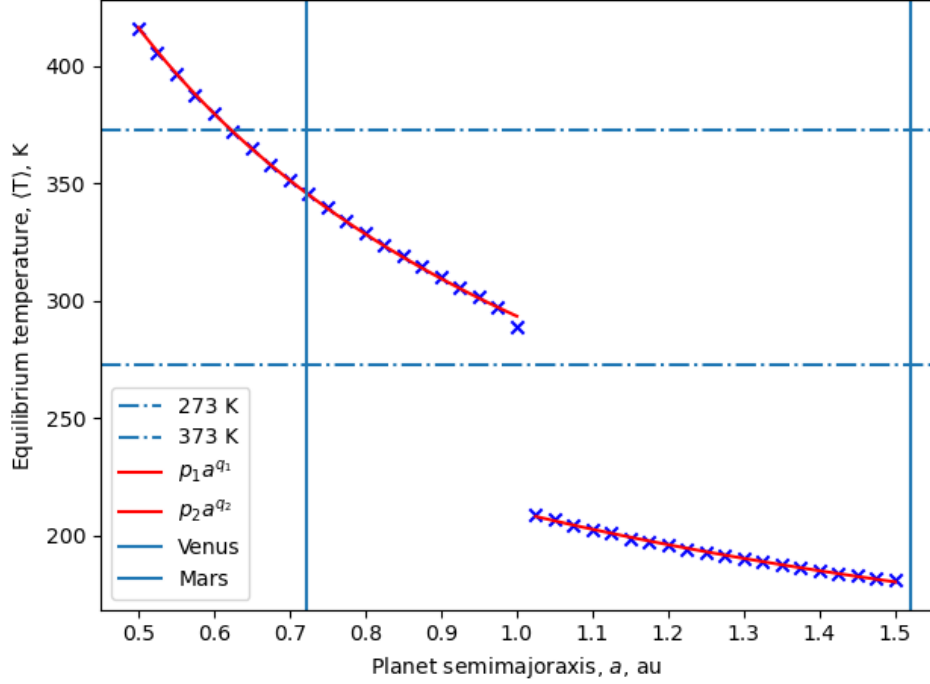
FIG. 3: A plot of the equilibrium temperature of the planet when varying its semimajor axis at constant eccentricity of $e = 0.0167$. Overlaid on the plot are two curves which are fitted to the data by a least squares regression. The form of the curve is $\langle T \rangle = p_i a^{q_i}$. Also shown are the orbits of Venus and Mars to highlight the range of values considered.

with proportionality constant $(q_0(1 - A)/4\sigma)^{1/4} = 255$ K for an Earth-like albedo of 0.3.

The validity of this proportionality can be investigated in terms of the semimajor axis by keeping $e = 0.0167$ constant and varying a from just outside Mercury's orbit at 0.5 au to Mars' orbit at 1.5 au. As seen in Figure 3 there are three main zones of interest to consider.

The first zone with $a < 0.65$ au has temperatures too high to sustain liquid water due to being too close to the Sun. The second zone with $0.65 < a < 1$ au is much more temperate, and is able to sustain liquid water on the planet's surface. Both the first and second zones are described by $\langle T \rangle = p_1 a^{q_1}$ with $p_1 = 293.5 \pm 0.4$ and $q_1 = -0.505 \pm 0.004$. q_1 is very close to the expected -0.5 powerlaw seen in eq. (31). However, the value of p_1 is 38 K higher than the expected proportionality, most likely due to the additional greenhouse effect present in the 1D model.

The third zone with $a > 1$ au is a sudden departure from this expected powerlaw, with $p_2 = 210.2 \pm 0.2$ and $q_2 = -0.378 \pm 0.003$. This is due to ice-albedo feedback which works as follows. As the planet cools, ice forms with a higher albedo than the land or ocean. This higher albedo means more light is reflected, thus the planet absorbs less heat, so cools more. This cycle continues until the planet reaches a much colder equilibrium than is expected by a fixed albedo method. At 1 au the planet is on a tipping point in terms of this feedback loop, as seen by the temperature being slightly lower than expected by eqn. (31). This, along with the following analysis of eccentricity and obliquity, help show why the Earth has had many ice ages in the past [20].

FIG. 4: A plot of the equilibrium temperature of the planet when varying its eccentricity at constant semimajor axis of $a = 1$ au. Overlaid on the plot is a curve which is fitted to the data by a least squares regression. The form of the curve is $\langle T \rangle = p(1 - e^2)^{-1/8}$. Also shown are the current and maximum theoretical value of Earth's eccentricity [18]. The minimum value is 0. There is a dip from the model at lower eccentricities due to ice-albedo feedback forming polar icecaps.

Alternatively, a can be fixed at 1 au and the eccentricity can be varied from a perfect circle, $e = 0$, to a very eccentric ellipse, $e = 0.9$. Beyond $e > 0.9$ the iteration to find orbital distance converges much less quickly so becomes intractible. Additionally planets in extreme orbits with $e > 0.9$ would be extremely unstable and most likely would not be able to retain an atmosphere due to extreme temperatures.

Varying the eccentricity is similar to varying the semimajor axis. There are two main zones of interest in Figure 4 where the eccentricity of the planet is varied.

The zone with $e > 0.2$ follows the relationship well, and the globally averaged temperature doesn't exceed the boiling point of water. On the other hand, the zone with $e < 0.2$ is up to 5 K lower than the relationship. This dip is again due to ice-albedo feedback. High eccentricities mean the planet gathers and stores enough thermal energy when close to the Sun to prevent polar ice caps from forming even when further away from the Sun. Lower eccentricities allow for polar ice caps to form which then significantly lower the global temperature.

As seen from the vertical lines in Fig. 4, the Earth has moved in this lower eccentricity region for its entire history, suggesting that the presence of the polar caps has been reasonably constant for the recent past.

13
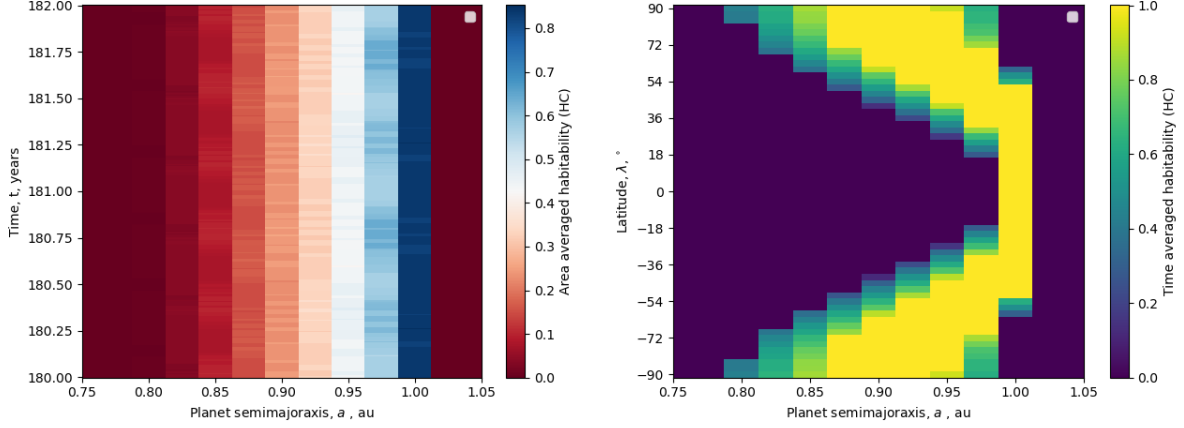
FIG. 5: Left: A heatmap for area-averaged HC habitability for a 2 years on the y-axis and planet semimajor axis between 0.75 and 1.05 au on the x-axis. The planet is never 100% habitable, reaching a maximum of 85% when at the Earth-like 1 au. Right: A heatmap for the 10-year time-averaged HC habitability for each latitude band on the y axis and the same planet semimajor axis values on the x-axis. In this case some latitude bands do reach 100% habitability.
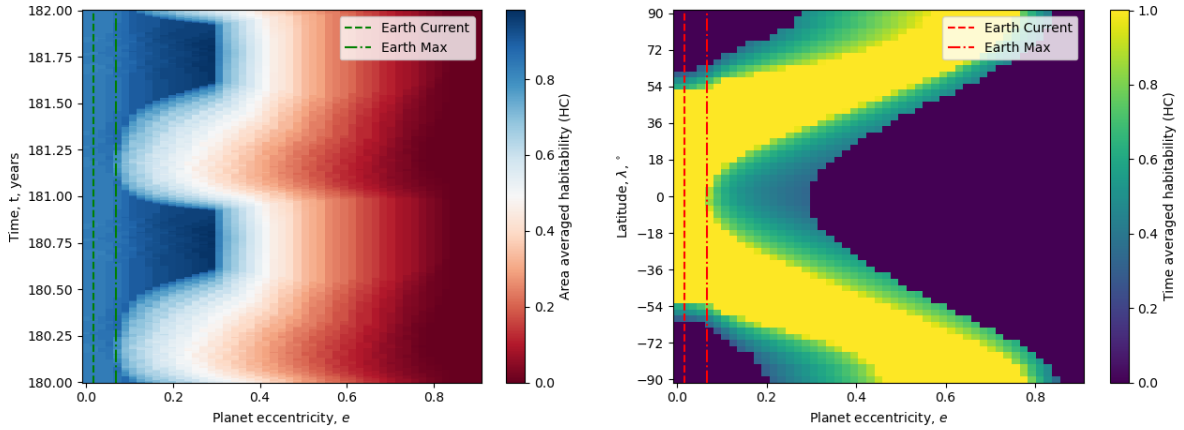

FIG. 6: Left: A heatmap for area-averaged HC habitability for a 2 years on the y-axis and planet eccentricity between 0 and 0.9 on the x-axis. The planet is never 100% habitable, reaching a maximum of 85%. Right: A heatmap for the 10-year time-averaged HC habitability for each latitude band on the y axis and the same planet eccentricity values on the x-axis. As eccentricity increases the habitable zones of the planet move outwards towards the poles because they are less directly insolated.

B. Semimajor axis and eccentricity

In Fig. 5 the semimajor axis of the planet is varied between just outside Mercury's orbit and Mars' orbit at constant eccentricity in order to investigate how HC habitability changes. The area-averaged habitability shows slight variations in habitability over time. This variation occurs for two main reasons: the growth and recession of the polar icecaps and equatorial desert. This growth and recession is shown in the time-averaged habitability where polar and equatorial regions have habitabilities between 0 and 1, indicating they are partially habitable over time.

As a decreases from 1 au, the planet experiences higher insolation. This higher insolation
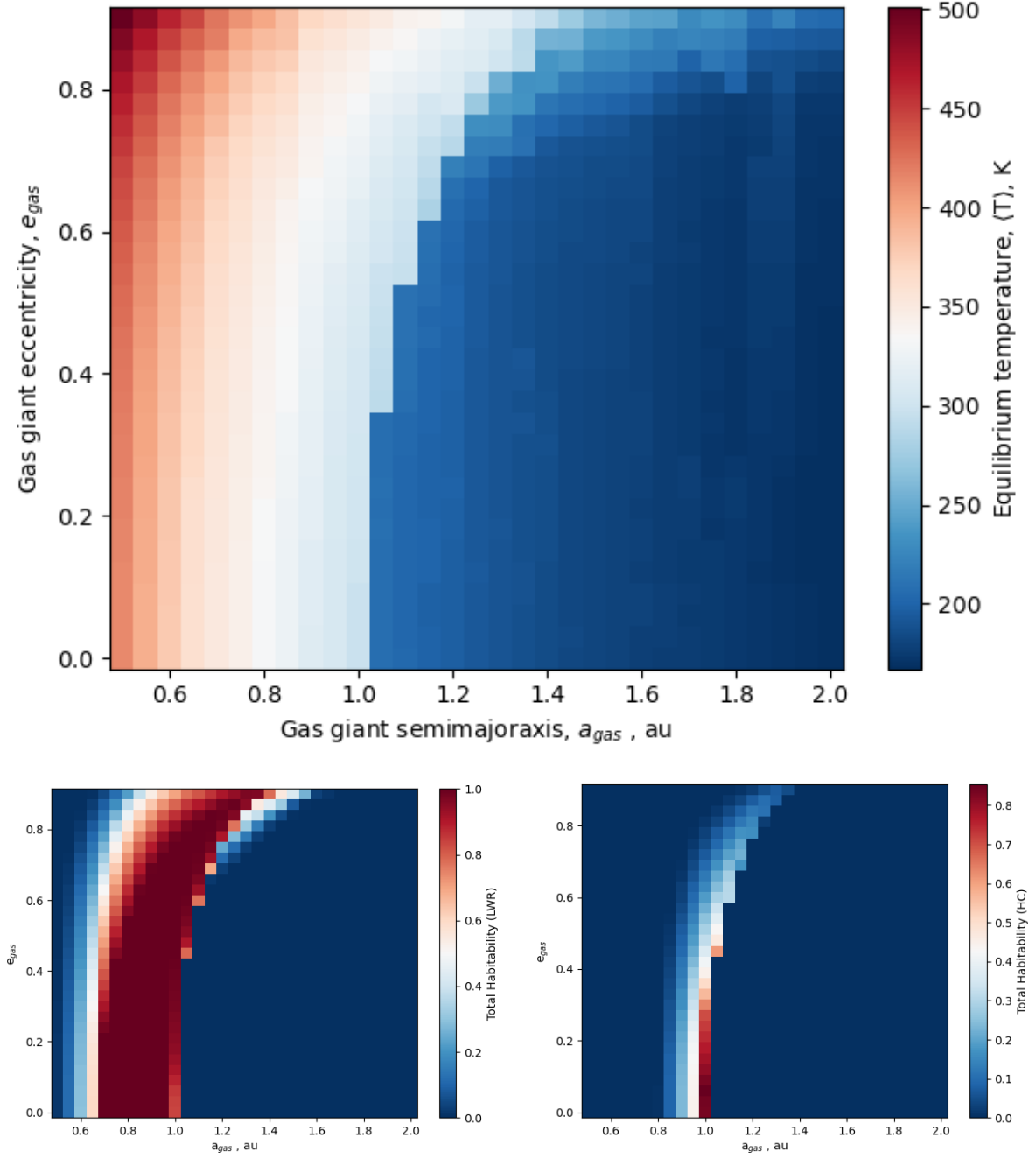
FIG. 7: Top: Varying the semimajoraxis and eccentricity of the gas giant to produce a heat map for the equilibrium temperature of the planet. Left: Processing of the temperature data with eqn. (19). Right: Processing of the temperature data with eqn. (20).

gives rise to higher temperatures across the planet. This melts the poles which are otherwise frozen, and causes the already hot equator to become too hot to sustain life.

Slightly increasing a from 1 au, the planet experiences a sharp drop in temperature. This is due to ice-albedo feedback where a small temperature decrease allows the icecaps to grow, and further decrease insolation until the entire planet is covered in ice.

In this case the HC habitability means that an Earth-like planet would not be habitable at the orbits of our closest neighbours, Venus and Mars.

Similarly, Fig. 6 shows the effects on habitability when the eccentricity of the planet is varied from 0 to 0.9. At low eccentricities, such as those the Earth has experienced in it's history, there is little variation both in area- and time-averaged habitabilites.

Increasing eccentricity results in more seasonality. For example for $e = 0.2$ the planet has an area averaged habitability which starts at 0.5, increases to 0.85, then decreases again at the turn of the year. This is because the planet's temperature is too hot in the first half of the year near the Sun, and is temperate all over the planet for the other half of the year as the planet is allowed to cool away from the Sun. However for eccentricities $e > 0.3$ the hot spike as the planet is close to the Sun exceeds the maximum limit and latitude bands at the equator are considered fully uninhabitable. This results in a sizeable decrease in habitability for the other half of the year where the planet is cooling.

At extreme values of eccentricity, only the poles stay cool enough year round to harbour life. However, this represents a small fraction of the surface area of the planet. At eccentricites above $e > 0.8$ the poles become too hot for life at certain parts of the year, and eventually are totally uninhabitable.

So far the semimajor axis and eccentricity have been varied independently to investigate effects on the time and area habitabilites. Varying both together can illuminate the habitability parameter space for orbits in exoplanet systems. This is shown in Fig. 7 where the semimajor axis and eccentricity of a planet are varied together. The top graph is a heatmap for the equilibrium temperature of the planet, and the bottom graphs are the processing of the temperature data using the LWR habitability and HC habitability which are then time and area averaged.

The temperature heatmap highlights the drop off in temperature when ice-albedo feedback starts and the planet falls into a snowball. There exist some above freezing temperatures for high eccentricity and high semimajor axis, likely due to the planets unfreezing when close the Sun, and refreezing when further away.

Both habitabilites show similar shapes with different widths which is reflective of HC being more restrictive in temperature range than LWR. The differnce in the habitabilites is shown at high eccentricity. The LWR habitability suggests that there is a wide range of semimajor axis values where liquid water exists on the surface of the planet year-round at high eccentricities. Alternatively, the HC habitability indicates that high eccentricities have extremes of temperature which are not compatible with life, thus the actual habitability is lower.
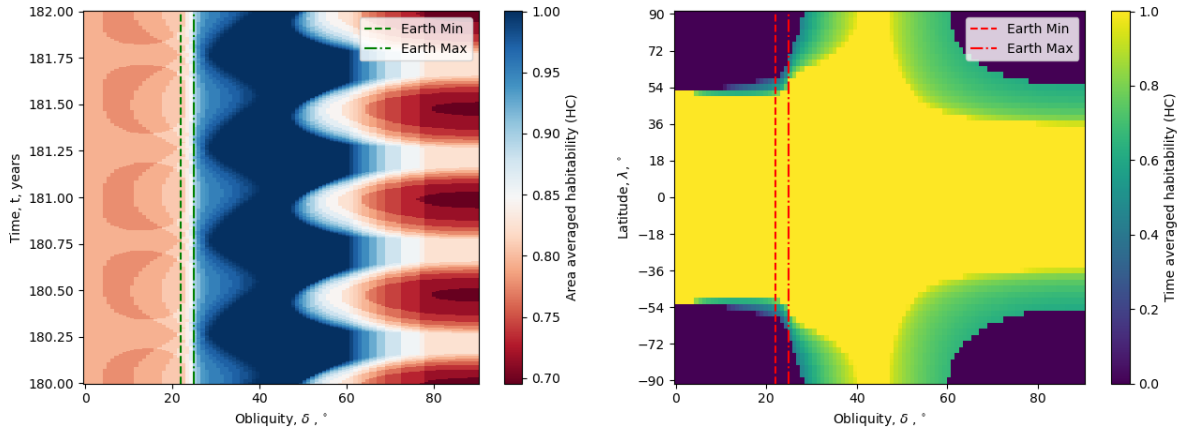
C.   Obliquity

The obliquity of the planet's spin can be varied to see how the habitability profile changes. Due to the uniform nature of the planet there is a symmetry about $\delta = 90°$. Because of this symmetry only values between $0°$ and $90°$ need to be considered.

Varying obliquity is shown in Fig. 8. There are three main areas to consider:

- Low obliquity ($0° - 20°$) where the planet directly presents its equator to the Sun for the majority of it's orbit.

- Medium obliquity ($20° - 50°$) where the planet presents both the equator and poles to the Sun in roughly equal amounts.

FIG. 8: Left: The area-averaged human habitability for a 2 year period after 150 years of simulation. The habitability varies between 70% and 100%, with the highest habitabilities being between 20°and 50°At lower obliquities polar ice caps form reducing the area habitability. Right: The 10 year time-averaged human habitability for each latitude band. Habitability at the equator of this planet is usually totally habitable all year around.

- High obliquity $(50° - 90°)$ where the planet cycles between presenting a pole to the Sun and presenting the equator (sideways) to the Sun.

For low obliquities there are small habitability variations. These variations are due to the permanent icecaps growing and shrinking. As the cap grows more latitude bands are below freezing so area-averaged habitability decreases. As the cap shrinks the opposite occurs, and area-averaged habitability increases. At especially low obliquities the shrinking and growing is smaller than the width of a latitude band so the habitability is constant.

At medium obliquities the icecaps are insolated directly enough to be melted. At the lower end of this range the icecaps can reform for the portion of the year that they are facing away from the Sun, and then melt in the portion of the year when facing toward the Sun. This results in some seasonal habitability. In the middle of this range the poles are melted for the entire year. This suggests an optimal range for obliquity where the insolation is spread out evenly across the planet, allowing for the entire surface to be temperate (and thus habitable) for all time.

At very high obliquities each pole is either directly insolated or in shadow for long periods of time, so experience extreme temperatures. The pole which is being directly insolated becomes very hot and can exceed the maximum temperature which sets the habitability of the latitude band to 0 for all time. Conversely, the pole which is in constant shadow quickly cools and freezes over. This exceeds the minimum temperature for habitability. Between the poles is a steep temperature gradient from hot to cold pole. This gives rise to the 80% habitability regions between dark spots where the habitability is at its highest for large obliquity.

As the planet moves in the orbit the equator is directly insolated and both poles are only partially insolated. The equator has a much larger area so can distribute this extra heat better so exceeds the habitable limit but not the maximum temperature. The poles at this time are able to melt or cool as appropriate. While the temperatures they reach at this time may be suitable for life, they exceeded the maximum limit so are still considered uninhabitable. The overall effect are seen in the darker 70% habitable regions where the poles and equator both have reduced

17
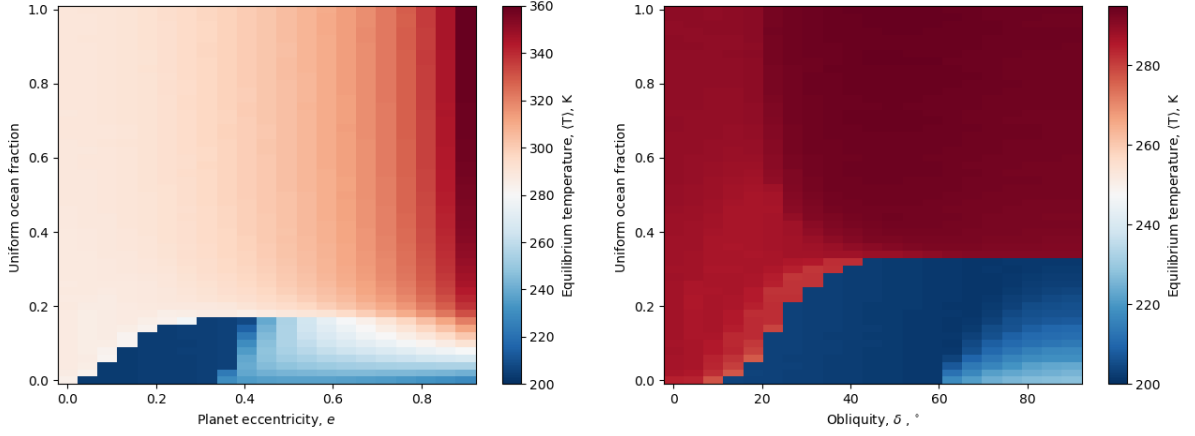
FIG. 9: A heatmap for equilibrium temperature when varying ocean fraction with eccentricity (Left) and obliquity (Right). The two main regions in both graphs are the warm temperatures with higher ocean fraction and much colder temperatures with lower ocean fractions. While both temperature scales start at 200 K, the eccentricity graph reaches 360 K whereas the obliquity graph reaches 295 K.

habitability.

Most planets have obliquities which can vary through this entire range of values. The Earth is an exception to this. The Moon stabilises the Earth's obliquity to vary between $22°$ and $25°$ with a current value of $23.5°$ (decreasing). In this range the habitability is fairly constant.

D.   Ocean fraction

The snowball state produced by ice-albedo feedback has been seen when varying semimajor axis (Figs. 3 and 5) and partially when varying eccentricity (Fig. 4). A variable which influences susceptibility to ice-albedo feedback is the ocean fraction.

The thermal timescale is defined as the time taken to emit all the energy in a latitude band via IR emission,

$$\tau = \frac{CT}{I} \tag{32}$$

This means that ocean, which has a higher heat capacity than land, has a larger thermal inertia. Larger thermal inertia means the ocean on the planet helps to reduce temperature variations which the planet experiences. Thus it is expected that planets with low ocean fraction will be susceptible to ice-albedo feedback in shorter timescales or with less forcing than high ocean fraction planets. The main variables influencing this forcing are the eccentricity and obliquity.

In an eccentric orbit the insolation decreases as the planet moves away from the Sun. This reduced insolation causes a lower temperature for a portion of the year. If the temperature is reduced enough, ice-albedo feedback can kick in and cause the planet to fall into a snowball state that it cannot recover from.

Obliquity can also cause snowball states. Obliquity for the Earth means seasons, where winter occurs in a hemisphere when that hemisphere points away the Sun because it is less directly insolated. The severity of this winter depends on how much of the pole is in permanent shadow and how long the winter lasts. Permanent shadow is influenced by the obliquity of the

planet, and the length of the winter depends on the period of the orbit. Varying obliquity will allow for the investigation of the permanent shadow effect.

To investigate these expectations the ocean fraction of the model is varied in Fig. 9. In the left plot ocean fraction is varied against eccentricity with zero obliquity, and in the right plot ocean fraction is varied against obliquity with zero eccentricity.

We see that for eccentricity there as a minimum ocean fraction which increases with eccentricity until a maximum at $e = 0.3$ of $f_{\text{ocean}} = 20\%$. At $e = 0$ there is no temperature variation, so the model cannot fall into a snowball state. As eccentricity increases the minimum ocean fraction, thus minimum thermal inertia, required to prevent a fall into a snowball state increases as expected. Unexpected is the region after $e > 0.4$.

At much higher eccentricities and low ocean fraction the planet moves further from the Sun so falls into a snowball state more easily. It can also move closer to the Sun which then increases the insolation. This insolation can be higher enough to allow the planet to melt and leave the snowball state. The combination of these two effects is that the planet is very hot half of the year and frozen for the other half of the year, with an average temperature which is habitable.

The habitability of this sort of planet is difficult to quantify. Humans have survived iceages in the past by burning fuels and sheltering in caves, to give just two examples. We are yet to see if human life will survive extreme heat.

In a similar way when varying obliquity the minimum ocean fraction starts at 0 and increases until a maximum at roughly $\delta = 45°$. For $0° < \delta < 10°$ the planet does not fall into a snowball state as the permanent shadow region is not large enough to cause runaway ice-albedo feedback.

For Earth-like obliquities (between $22°$ and $25°$) the planet is susceptible to a snowball state only if the planet has ocean fraction less than roughly 15%.

At very high obliquities (and low ocean fractions) the pole which faces the Sun can be melted. This is because low ocean fraction has low heat capacity, so the heat input from the direct insolation to the polar region can raise the temperature of the region very easily. This is very localised to the polar region and so only slightly raises the average temperature of the planet.

The minimum ocean fraction for the obliquity case is much larger than the eccentricity case. This is indicative that the temperature variations due to obliquity are much larger than variations due to eccentricity. This is likely due to the obliquity having a more localised effect on the polar regions of the planet as opposed to eccentricity's planetwide effect.

Both variables cause the planet to be susceptible to ice-albedo feedback, and both cause full or partial recovery from snowball at extreme values. For eccentricity the minimum ocean fraction varies approximately quadratically with eccentricity until $e = 0.4$ where the eccentricity is high enough to melt the induced snowball meaning the time averaged temperature increases. The minimum ocean fraction in the obliquity case varies with an 'S' shape and levels out after $\delta = 40°$ to a minimum ocean fraction of $f_{\text{ocean, min}} = 0.36$. Similar to the eccentricity case, high obliquities can partially recover from the snowball. In this case it is due to the pole facing the Sun melting for half a year due to constant insolation before refreezing when facing away from the Sun. There are nearly no variations due to changing ocean fraction above $f_{\text{ocean}} = 0.2$ in the eccentricity case, and few variations above $f_{\text{ocean}} = 0.4$ for the obliquity case.
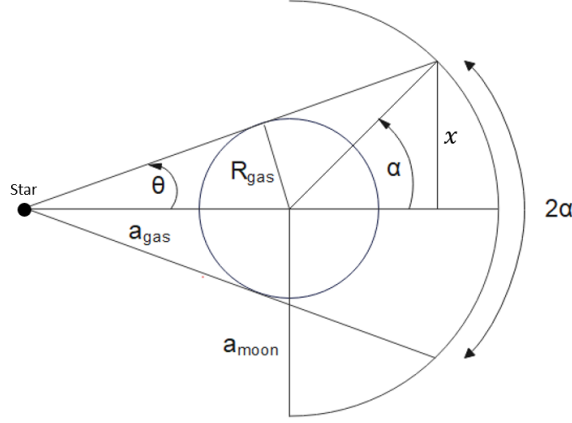
FIG. 10: A diagram of a planet in orbit around a star at a distance a_{gas}, and a moon in orbit of the planet at a distance a_{moon}. The planet has radius R_{gas}. The angle 2θ corresponds to the angular size of the planet from the star. Inside the angle 2α the moon is eclipsed by the planet.
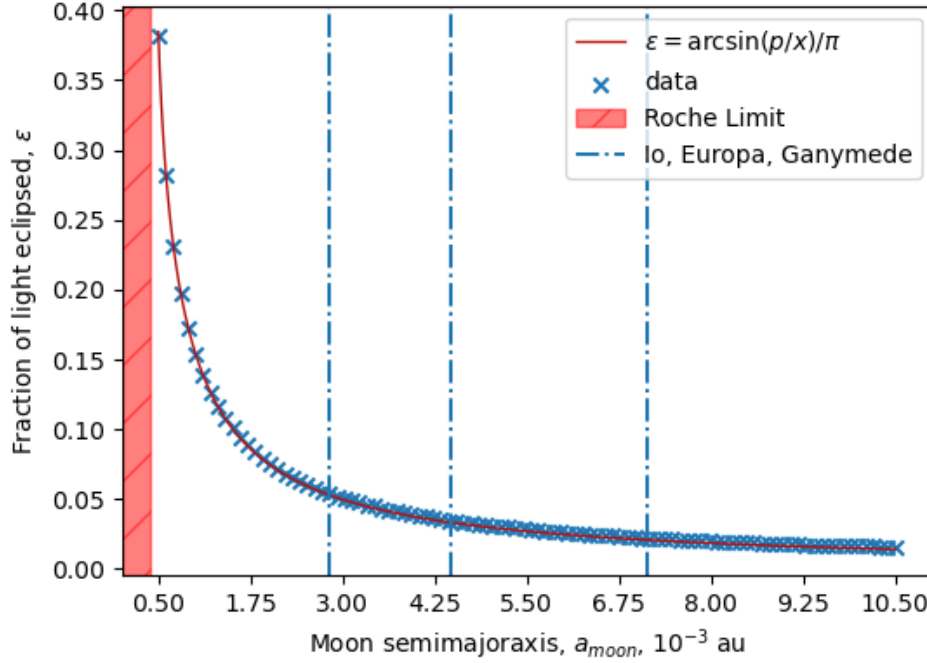
FIG. 11: Fraction of light eclipsed by a Jupiter sized gas giant when varying a moon's semimajor axis. Shown is the Roche limit for Jupiter, as well as the orbital distances of Jupiter's three innermost moons. Overlaid on the data is a fit of $\epsilon = \arcsin(p/x)/\pi$ with parameter $p = (4.675 \pm 0.005) \times 10^{-4}$ au.

6. EXOMOONS

A. Eclipsing

planet and moon orbits are (close to) co-planar. this means eclipsing quantify eclipsing using 2 independent 2-body solutions (distance (28), angle (29)) - requires timesteps of 1 hour as eclipses are very short this establishes that eccentricity of the planet orbit has negligible effect.

eccentricity of the moon as small effect (1%) semimajor axis of the planet also small Largest contributor is moon semimajor axis

evolving the 2 independent solutions in parallel with the EBCM is impractical knowing that both eccentricities have very small effects leads to the setup for an analytical solution for circular orbits. 10 where the sun has been assumed to be a point source (i.e. if $a_{\text{gas}} \gg 10 * a_{\text{moon}}$)

Eclipsing of the moon by the gas giant was initially investigated by finding the orbital distance and angle for gravitational attraction which showed that varying the eccentricity of the moon or planet resulted in no change to time-averaged eclipsing fraction. Thus, the main influences of eclipsing are gas giant semimajor axis and moon semimajor axis, with moon semimajor axis being the most important factor.

In order to add eclipsing to the EBCM without running the 2-body solution in parallel, the eclipsing fraction must be quantified. To do this the star is assumed to be a point source, and both planets are assumed to be in circular orbits which are coplanar. Figure 10 shows the configuration of the system, including the angle 2α which is the fraction of the moon's orbit which is spent being eclipsed.

α can be related to the length x by

$$\sin \alpha = \frac{x}{a_{\text{moon}}}, \tag{33}$$

θ can be related to the length x by

$$\sin \theta = \frac{x}{a_{\text{gas}} + a_{\text{moon}} \cos \alpha} = \frac{R_{\text{gas}}}{a_{\text{gas}}}, \tag{34}$$

combining eqns. (33) and (34) leads to

$$(a_{\text{gas}} + a_{\text{moon}} \cos \alpha) \frac{R_{\text{gas}}}{a_{\text{gas}}} = a_{\text{moon}} \sin \alpha, \tag{35}$$

thus

$$\frac{R_{\text{gas}}}{a_{\text{moon}}} = \sin \alpha - \frac{R_{\text{gas}}}{a_{\text{gas}}} \cos \alpha, \tag{36}$$

α can be solved for by approximating $R_{\text{gas}} \ll a_{\text{gas}}$. Dividing 2α by the full 2π angle the moon rotates through, the eclipsing fraction can be found as

$$\epsilon = \frac{2\alpha}{2\pi} = \frac{\arcsin(R_{\text{gas}}/a_{\text{moon}})}{\pi}, \tag{37}$$

for a planet of radius R_{gas} and moon semimajor axis a_{moon}.

This relation is investigated in Fig. 11 with a free parameter in place of R_{gas}. The value of the free parameter is $(7.013 \pm 0.008) \times 10^7 \text{m}$ which is extremely close to the radius of Jupiter, as to be expected.

B.   Tidal heating

Tidal heating occurs when the core of the moon is compressed and relaxed by unequal gravitational forces as the moon moves through an elliptical orbit. Segatz et al 1988 [22] provide

Moon				Gas Giant		
Semimajor axis	Eccentricity	Radius	Density	Mass	Radius	Albedo
0.03 au	0.006	6.4×10^6 m	5500 kg m^{-3}	1.9×10^{27} kg	7.0×10^7 m	0.3

TABLE II: A summary of the default parameters for the Earth-like exomoon model. The moon orbital parameters are ones which generate a good level of tidal heating, and the radius and density are similar to the radius and density of the Earth. The gas giant parameters are the same as Jupiter's [21], where the volumetric mean radius, and bond albedo have been used. Other model parameters are the same as the planetary model (Tab. I).

models for the tidal heating in terms of both a 'fixed-Q' model providing a constant tidal heating, and a suite of 'viscoelastic' models which account for conditions of the material within the moon.

The 'fixed-Q' model is given by

$$F_{\text{f-Q}} = \frac{21}{2} \frac{k_2}{Q} \frac{G^{3/2} M_{\text{gas}}^{5/2} R_{\text{moon}}^5 e_{\text{moon}}^2}{a_{\text{moon}}^{15/2}} \tag{38}$$

where k_2 is the second love number for the moon and Q is the total dissipation factor due to friction. this assumes only viscous heating (segatz about io, probably relevant)

The k_2/Q term is a collection of various viscosity and shear modulus terms which are assumed to be constant. The model can be made more dynamic by replacing these constant terms with the imaginary part of the second-order Love number, $-\text{Im}(k_2)$:

$$F_{\text{VE}} = -\frac{21}{2} \text{Im}(k_2) \frac{G^{3/2} M_{\text{gas}}^{5/2} R_{\text{moon}}^5 e_{\text{moon}}^2}{a_{\text{moon}}^{15/2}} \tag{39}$$

where an anelastic Maxwell model is used to give the imaginary part of the second-order Love number as

$$-\text{Im}(k_2) = \frac{57 \eta \omega}{4\beta \left[1 + \left(1 + \frac{19\mu}{2\beta}\right)^2 \left(\frac{\eta\omega}{\mu}\right)^2 \right]} \tag{40}$$

where $\beta = \rho g R_{\text{moon}}$ has been described as gravitational stiffness term [23]. The temperature dependent forms of the viscosity, η, and shear modulus, μ, are given in Henning et al [23] and in appx. B. The orbital frequency, density, and radius of the moon are ω, ρ, and R_{moon} respectively, with default values in table II.

[24] [25]

C. Results

With the model appropriately updated, temperature profiles and habitabilities seen previously can be investigated for this moon model. Shown in Fig. 12 is how the time-averaged (HC) habitability for variable semimajor axis changes between the planetary model and moon model (left) and how the equilibrium temperature changes with semimajor axis (right). The plot on the left shows how the latitude habitable zone changes between a planetary model and
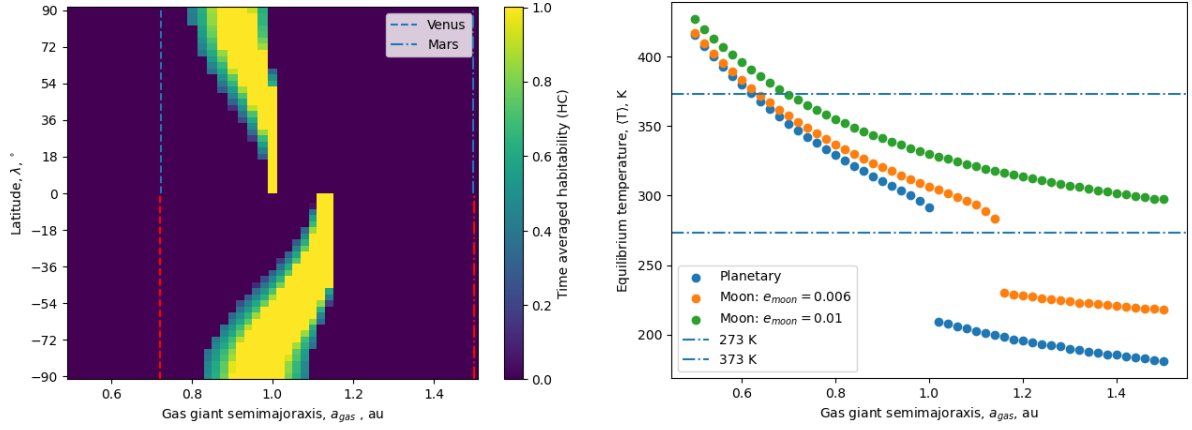
FIG. 12: Left: Comparison of the time-averaged (HC) habitability for variable semimajor axis for the planetary model (top) and moon model (bottom). The moon model has the default parameters in Tab. II. Right: Comparison of the equilibrium temperatures when varying gas giant semimajor axis for the planetary model (blue), and two moon models with different eccentricity (orange and green). Also shown are horizontal lines for the freezing and melting points of water.

a moon model with the default parameters in Tab. II. And the plot on the right shows how the equilibrium temperature of the planet between the planetary model and two moon models, one with default parameters and one with higher eccentricity.

The habitable zone becomes wider at all latitudes and moves outwards towards Mars' orbit. The reason for both these effects is the additional energy flux from tidal heating. The habitable zone becomes wider as the moon is less reliant on a specific distance from the Sun to generate habitable temperatures. The habitable zone moves further out as the additional energy flux generally raises the temperature of the planet, meaning it is too hot for life at the closer distances.

This is also seen in the equilibrium temperatures, where a wider range of values are within the range for liquid water. Seen in the orange set of data is a more exaggerated curve when falling to the snowball state than for the planetary model in blue. This is due to ice-albedo feedback playing less of a role in determining the climate of the planet as the tidal heating is independent of albedo. The tidal heating also helps to prevent the planet's temperature from decreasing to the point where ice-albedo feedback can dominate by providing a constant heat source when further from the star.

eccentricity: The temperature generally increases. The dip at low eccentricity due to ice-albedo feedback is missing from the moon models. This is due to the generally higher temperature

obliquity: Temperature increases. Temperature range decreases due to insolation playing smaller role (proportionally) in determining the planet climate. The variations due to obliquity become smaller as any insolation variation across the planet are dampened by the uniform tidal heating.
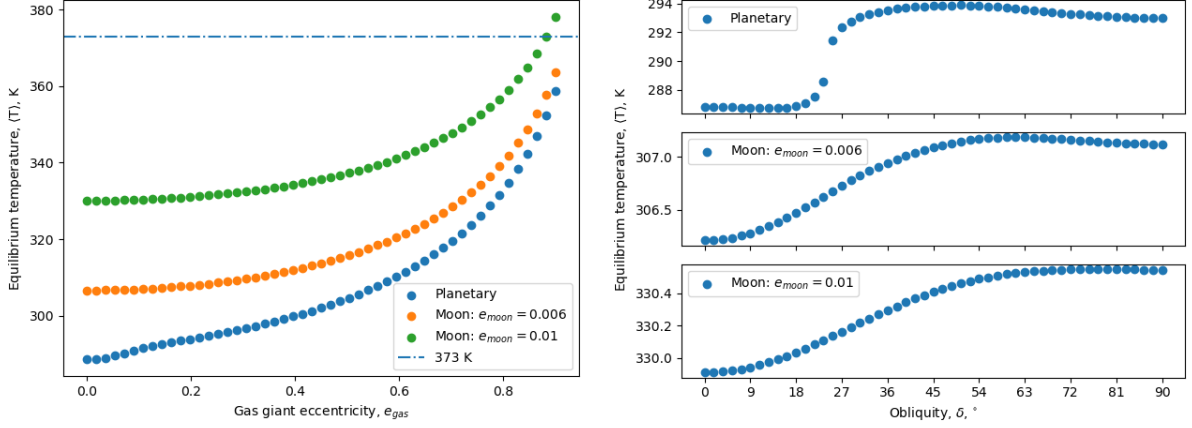
FIG. 13: Left: Comparison of the equilibrium temperatures when varying gas giant eccentricity for the planetary model (blue), and two moon models with different eccentricity (orange and green). Right: Comparison of the equilibrium temperatures when varying obliquity for the planetary model (top), and two moon models with different eccentricity (middle and bottom). The y-axes are very different, as each has progressively smaller range in values.

7.   DISCUSSION

Research motivated by climate change suggests that ice melting can release CO_2 which is not accounted for in this model. This would introduce a ice-temperature feedback where melting ice releases CO_2, increasing greenhouse gas effects and feeding back until the temperature is very high. This would reduce the habitability at higher temperatures particularly where the icecaps melt due to a higher CO_2 fraction in the atmosphere, thus larger greenhouse effect. However this effect is very particular for the Earth due to it's CO_2 rich past. It would not be correct to assume that all exoplanets have a CO_2 rich past but could be considered in further research.

Ice melting and rising temperatures would also cause the oceans to expand, thus changing the mixing depth (thus heat capacity) of the oceans.

The approximation of a uniform planet could also be probed further. Exoplanets may have land-ocean distributions similar to Earth where the northern hemisphere has more land than the southern hemisphere. The planet could be probed with different fractions of land and ocean. For example: an ocean centered on one of the poles of the planet and increasing in size from a desert world with small a polar ocean to ocean world with a small polar continent.

8.   CONCLUSION

REFERENCES

[1] ESA, "A brief introduction to exoplanets." https://sci.esa.int/web/exoplanets/-/60654-a-brief-introduction-to-exoplanets. Accessed: 2024/03/05, Last updated 2019/09/01.

[2] D. N. et al, "KOI-142, The king of transit variations, is a pair of planets near the 2:1 resonance," ApJ, vol. 777, no. 1, 2013.

[3] K. Lewis and et al, "Possibility of detecting moons of pulsar planets through time-of-arrival analysis," ApJ, vol. 685, no. 2, 2008.

[4] D. Kipping, S. Fossey, and G. Campanella, "On the detectability of habitable exomoons with kepler-class photometry," RAS, vol. 400, no. 1, 2009.

[5] M. Limbach and E. Turner, "On the direct imaging of tidally heated exomoons," ApJ, vol. 769, no. 2, 2013.

[6] M. Limbach and et al, "On the detection of exomoons transiting isolated planetary-mass objects," ApJ, vol. 918, no. 2, 2021.

[7] Exoplanet Team. `https://exoplanet.eu`. Accessed: 2024/03/05, Last update: 2024/03/04.

[8] NASA, "Artemis plan." `https://www.nasa.gov/specials/artemis/`. Accessed: 2024/03/06.

[9] CNSA, "China and russia sign a memorandum of understanding regarding cooperation for the construction of the international lunar research station." `https://www.cnsa.gov.cn/english/n6465652/n6465653/c6811380/content.html`. Accessed: 2024/03/06.

[10] M. Gillon, A. Triaud, B. Demory, and etal, "Seven temperate terrestrial planets around the nearby ultracool dwarf star TRAPPIST-1," Nature, vol. 542, 2017.

[11] O. C. et al, "Heating of the atmospheres of short-orbit exoplanets by their rapid orbital motion through an extreme space environment," ApJ, vol. 962, no. 2, 2024.

[12] G. V. L. etal, "Airy worlds or barren rocks? on the survivability of secondary atmospheres around the TRAPPIST-1 planets," A&A, 2024. Awaiting Publication, `https://doi.org/10.48550/arXiv.2401.16490`.

[13] North and Coakley, "Differences between seasonal and mean annual energy balance model calculations of climate and climate sensitivity," J. Atmos. Sci., vol. 36, no. 7, 1979.

[14] Williams and Kasting, "Habitable planets with high obliquities," Icarus, vol. 129, no. 1, 1997.

[15] D. Spiegel and et al, "Habitable climates," ApJ, vol. 681, no. 2, 2008.

[16] D. Spiegel and et al, "Habitable climates: the influence of obliquity," ApJ, vol. 691, no. 1, 2009.

[17] C. Dressing and et al, "Habitable climates: the influence of eccentricity," ApJ, vol. 721, no. 2, 2010.

[18] J. Laskar, A. Fienga, M. Gastineau, and H. Manche, "La2010: a new orbital solution for the long-term motion of the earth," A&A, vol. 532, 2011.

[19] A. Méndez and E. Rivera-Valentín, "The equilibrium temperature of planets in elliptical orbits," ApJL, vol. 837, no. 1, 2017.

[20] C. Emiliani, "The cause of the ice ages," Earth and Planetary Science Letters, vol. 37, 1978.

[21] NASA, "Jupiter fact sheet." `https://nssdc.gsfc.nasa.gov/planetary/factsheet/jupiterfact.html`. Accessed: 2024/03/01.

[22] Segatz and et al, "Tidal dissipation, surface heat flow, and figure of viscoelastic models of io," Icarus, vol. 75, no. 2, 1988.

[23] W. G. Henning and et al, "Tidally heated terrestrial exoplanets: viscoelastic response models," ApJ, vol. 707, no. 2, 2009.

[24] V. Dobos, R. Heller, and E. Turner, "The effect of multiple heat sources on exomoon habitable zones," A&A, vol. 601, no. 91, 2017.

[25] M. Rovira-Navarro and et al, "Tidally heated exomoons around gas giants," Planet. Sci. J., vol. 2, no. 3, 2021.

Appendix A: Numerical stability of the 1D EBCM

Appendix B: Tidal heating equations and method

SCIENTIFIC SUMMARY FOR A GENERAL AUDIENCE

Many interesting solar systems have been reported in the news, such as the Trappist-1 system which is filled with Earth-like planets. Simulations and models such as those in this paper are used to determine if a planet could be habitable. A habitable zone can be made by varying the parameters of the model to see where the model is habitable, partially habitable, or uninhabitable.

The main model in this paper takes a planet and divides it into a number of latitude bands which can have energy flow between them. Certain parameters, such as how the planet orbits around its star and the angle the planet is tilted at, are varied to build this habitable zone. A result of this paper is if the Earth orbited slightly further away from the Sun then it is likely that it would fall into an ice age similar to what the Earth has experienced in the past. Another result found is that the tilt of the planet can affect how hot or cold it is, and indicates that the current tilt of the Earth gives a cold planet.

Another aspect of this paper's exoplanet research is exomoons orbiting a gas giant such as Jupiter. In certain configurations an exomoon can be heated not only from the host star, but also due to a process called tidal heating. Tidal heating is similar to stretching an elastic band. Stretching and relaxing an elastic band many times can cause the band to warm up. The moon of a gas planet is stretched slightly by unequal forces of gravity as one part of the moon is further away than the other. If the moon's orbit is not circular then the moon is stretched and relaxed, thus heats up in a similar way to the elastic band. Adding tidal heating to the model allows for investigations into how tidal heating can move, or change the shape of, the habitable zone.